loss occurs through diffuse fluid leakage. An accurate accounting of point-source heat losses could be used to gauge the scale of diffuse heat leakage where the total heat flux of a vent field was known.

For a nonconservative constituent, the advective transport in the plume equals that fraction of the original hydrothermal discharge which escapes the vent field (this fraction may be greater than 1 and may change with distance from the vent field, as for the particulate phase of a continually precipitating chemical species). The flux of total suspended particles through the northern boundary of the vent field, for example, was 94 ± 48 g/sec.

The flux of constituents that can be sampled only discretely may be estimated from their correlation with the continuously measured temperature or particle concentration. Samples of dissolved manganese (DMn) from throughout the plume, for example, exhibit a linear relation with ΔT (Fig. 3), giving a slope of 1.4 ± 0.1 nmol/cal and implying a total vent field flux of DMn of 0.2 ± 0.1 mol/sec. The DMn to heat ratios of high-temperature fluids at this site apparently range from 7.6 to 15.7 nmol/cal, however, because of extremely high concentrations of DMn [up to 4.5 mmol/kg (*14*)]. The approximate order of magnitude difference between DMn to heat ratios in the vent fluids and the diluted plume implies either that the reported high-temperature samples (*14*) are not representative of the integrated emissions of the entire vent field, or that 80 to 90% of the DMn is scavenged from the vent emissions during formation of the plume. Furthermore, the low and uniform particulate Mn in the plume (Fig. 3) requires that any scavenged Mn be deposited before the scavenging particles become entrained in the plume. Analogous inconsistencies have been observed near the 21°N vent fields, where the total dissolvable $Mn/^3He$ ratio in vent waters is about twice that in the plume waters (*15*).

Even though the origin of such inconsistencies is presently obscure, their existence indicates that a limited set of individual vent samples may not adequately represent the regional composition and flux of hydrothermal emissions. A regional view also clarifies the interpretation of time-dependent processes such as precipitation and scavenging in the plume, since samples collected along the advective path will appear to "age" much more slowly than samples collected across the plume boundaries. Finally, this approach can be readily expanded from vent-field to ridge-segment size, thereby enabling the measurement of hydrothermal flux on a spatial scale that will more appropriately reflect the scale of current geophysical models.

REFERENCES AND NOTES

1. R. F. Weiss, P. Lonsdale, J. E. Lupton, A. E. Bainbridge, H. Craig, *Nature (London)* **267**, 600 (1977); J. B. Corliss *et al.*, *Science* **203**, 1073 (1979); RISE Project Group, *ibid.* **207**, 1421 (1980); J. M. Edmond, K. L. Von Damm, R. E. McDuff, C. I. Measures, *Nature (London)* **297**, 187 (1982).
2. J. M. Edmond *et al.*, *Earth Planet. Sci. Lett.* **46**, 1 (1979); Canadian American Seamount Expedition, *Nature (London)* **313**, 212 (1985); K. L. Von Damm *et al.*, *Geochim. Cosmochim. Acta* **49**, 2197 (1985).
3. U.S.G.S. Juan de Fuca Study Group, *Geology*, in press.
4. K. C. Macdonald, K. Becker, F. N. Spiess, R. D. Ballard, *Earth Planet. Sci. Lett.* **48**, 1 (1980).
5. D. R. Converse, H. D. Holland, J. M. Edmond, *ibid.* **69**, 159 (1984).
6. J. R. Delaney, H. P. Johnson, J. L. Karsten, *J. Geophys. Res.* **86**, 11747 (1981); W. R. Normark, J. L. Morton, R. A. Koski, D. A. Clague, J. R. Delaney, *Geology* **11**, 158 (1985).
7. The instrument package consisted of a hydrodynamically faired Sea Bird CTD (conductivity-temperature-depth) coupled to a Sea Tech transmissometer with a 0.25-m path length. CTD resolution was ±0.00004 S/m and ±0.0003°C.
8. E. T. Baker, J. W. Lavelle, G. J. Massoth, *Nature (London)* **316**, 342 (1985).
9. Mean velocity along the plume axis is the component along 20° of the 2.86-hour-filtered 90-day current meter record. The standard error estimate is $\pm\sigma/(T/\tau)^{0.5}$, where σ = standard deviation of the current meter record, T = record length, and τ = an independent time scale [J. S. Allen and P. K. Kundu, *J. Phys. Oceanogr.* **8**, 13 (1978)] estimated as the area under the autocorrelation function for a particular record.
10. K. Crane *et al.*, *J. Geophys. Res.* **90**, 727 (1985).
11. J. L. Morton and N. H. Sleep, *ibid.*, p. 11345.
12. R. D. Ballard and J. Francheteau, *Mar. Tech. Soc. J.* **16**, 8 (1982).
13. K. C. Macdonald, *Annu. Rev. Earth Planet. Sci.* **10**, 155 (1982); N. H. Sleep, J. L. Morton, L. E. Burns, T. J. Wolery, in *Hydrothermal Processes at Seafloor Spreading Centers*, P. A. Rona, K. Bostrom, L. Laubier, K. L. Smith, Eds. (Plenum, New York, 1983), pp. 53–82.
14. K. Von Damm and J. L. Bischoff, *Eos* **66**, 926 (1985). The high end ratio was computed from the maximum DMn concentration and the single reported temperature of 284°C; the low end ratio from the minimum DMn concentration and the maximum expected temperature of 340°C.
15. J. E. Lupton *et al.*, *Earth Planet. Sci. Lett.* **50**, 115 (1980).
16. G. P. Klinkhammer, *Anal. Chem.* **52**, 117 (1980).

17. Supported by the NOAA VENTS program. We thank J. R. Delaney, S. Hammond, J. W. Lavelle, and H. Curl, Jr., for thoughtful reviews, and G. Lebon, K. Roe, and D. Tennant for technical assistance.

9 June 1986; accepted 6 October 1986

A Common Mechanism of Chromosomal Translocation in T- and B-Cell Neoplasia

LAWRENCE R. FINGER, RICHARD C. HARVEY, ROBERT C. A. MOORE, LOUISE C. SHOWE, CARLO M. CROCE

The chromosomal breakpoint involved in the t(8;14)(q24;q11) chromosome translocation in the SKW-3 cell line, which directly involves the 3′ flanking region of the c-*myc* gene, was cloned and sequenced. The breakpoint on chromosome 8 mapped to a position 3 kb 3′ of c-*myc* while the chromosome 14 breakpoint occurred 36 kb 5′ of the gene for the constant region of the α chain of the T-cell receptor (TCR). The translocation resulted in a precise rearrangement of sequences on chromosome 8 and what appears to be a functional J_α segment on chromosome 14. Signal sequences for V-J joining occurred at the breakpoint positions on both chromosomes 14 and 8, suggesting that the translocation occurs during TCR gene rearrangement and that it is catalyzed by the enzymatic systems involved in V-J joining reactions. The involvement of c-*myc* in the translocation and the association of joining signals at the breakpoints provides a parallel to the situation observed in the translocations involving c-*myc* and the immunoglobulin loci in B-cell neoplasms and suggests that common mechanisms of translocation and oncogene deregulation are involved in B- and T-cell malignancies.

MOST HUMAN T-CELL NEOPLASMS carry specific chromosomal rearrangements, predominantly chromosomal translocations and inversions. These rearrangements frequently involve chromosome 14 at band q11 (*1–4*) where the locus for the α chain of the T-cell receptor (TCR) resides. The α locus of the TCR (TCR-α) is split in T-cell leukemias carrying the t(11;14) chromosome translocation (*5*). The genes for the variable (V_α) regions are proximal to the breakpoints and remain on chromosome 14 while the gene for the constant region (C_α) translocates to chromosome 11 (*5*). In T-cell leukemias carrying a t(8;14)(q24;q11) chromosome translocation, the C_α locus translocates to a region 3′ to the c-*myc* oncogene (*6*). The translocation-associated c-*myc* gene is deregulated in Burkitt lymphomas (*7*) and a c-*myc* involved in a translocation with the TCR-α locus is similarly deregulated (*6*).

Both the t(11;14)(q13;q32) and the t(14;18)(q32;q21) chromosome translocations associated with specific B-cell neoplasms predominantly involve immunoglobulin heavy-chain J regions (*8*). In addition,

The Wistar Institute, Philadelphia, PA 19104.

sequences that are homologous to heptamer and nonamer joining signals have been identified on chromosomes 11 and 18 at the breakpoint positions, suggesting that enzymes involved in the immunoglobulin rearrangement may catalyze the translocations (*8, 9*). We present here the DNA sequence of the cloned breakpoint of a t(8;14)(q24;q11) chromosome translocation isolated from the SKW-3 leukemic T-cell line. This translocation involves a J region (J_α) of the TCR-α and V-J joining signals occur in the region of the breakpoint on both chromosomes 14 and 8.

The direct involvement of c-*myc* in the SKW-3 translocation was suggested by Southern blot analysis of digested SKW-3 DNA with a probe derived from the 3′ flanking region of c-*myc* (*10*), which revealed both normal and rearranged c-*myc* bands (Fig. 1). The chromosomal breakpoint was mapped to a region between the first Eco RI and the first Hind III site 3′ to the third *myc* exon. The increased intensity of the rearranged c-*myc* band in the SKW-3 DNA was due to the presence of two copies of the 8q+ chromosome in this cell line (*6*).

We have cloned the t(8;14) breakpoint from the SKW-3 cell line from a genomic DNA library constructed in the λ phage vector EMBL3A (*11*). Five overlapping phage clones that fully cover the c-*myc* locus were studied in detail. The restriction map analysis of the recombinant clones allowed

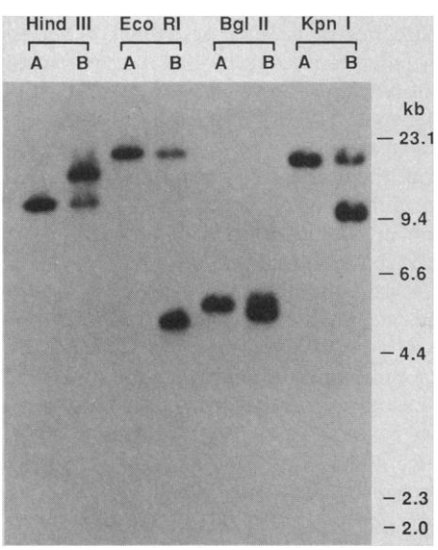

Fig. 1. Hybridization of DNA from the SKW-3 cell line to the 3′ c-*myc* probe pCA 1.7S. DNA's (10 μg) isolated from cells of (A) 697, a pre-B cell leukemia cell line used as a germline control, and (B) SKW-3 were cut with the restriction enzymes shown, separated on a 0.6% agarose gel, and transferred to a nitrocellulose filter. The Southern blot filter was hybridized in 50% formamide/4× standard saline citrate (SSC) at 37°C with ^{32}P-labeled probe and finally washed with 0.2× SSC at 65°C.

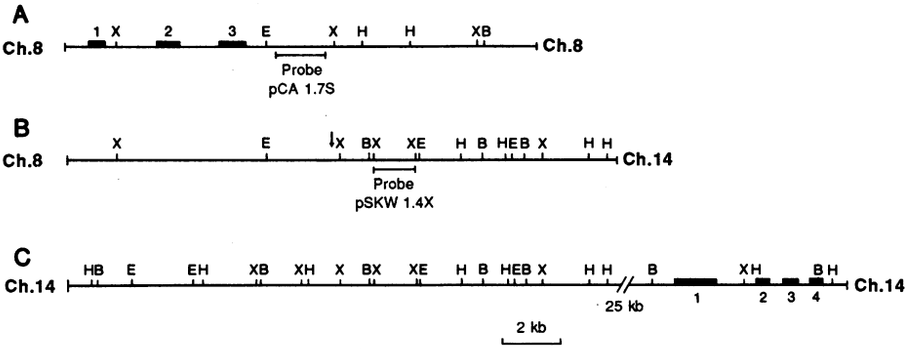

Fig. 2. Restriction maps of the regions surrounding the breakpoint in SKW-3. (A) The germline c-*myc* gene locus on chromosome 8. Exons of c-*myc* are indicated by numbered boxes 1, 2, and 3. (B) The rearranged c-*myc* locus on chromosome 8q+. The location of the breakpoint is shown by an arrow. (C) The germline α-chain locus on chromosome 14. Exons of the constant region are indicated by numbered boxes 1, 2, 3, and 4. The gap represents 25 kb of the J_α locus. E, Eco RI; B, Bam HI; H, Hind III; and X, Xba I.

their classification into two groups, having the germline *myc* locus on the normal chromosome 8 (Fig. 2A) or the rearranged c-*myc* locus on the 8q+ chromosome (Fig. 2B). The size of the rearranged SKW-3 DNA bands (Fig. 1) are in agreement with the calculated values for the appropriate restriction fragments in the rearranged clone. The position of the t(8;14) breakpoint is indicated on the map where the restriction map diverges from the germline configuration of the c-*myc* locus. A 1.4-kb Xba fragment that is 3′ to the mapped position of the breakpoint and that is free of repetitive sequences was isolated to confirm the derivation of this region from chromosome 14. The pSKW 1.4X probe (Fig. 2B) was used in Southern blot hybridization of DNA from rodent × human hybrid cells containing either human chromosome 8 or human chromosome 14. The pSKW 1.4X probe hybridized to DNA's from hybrids that only contain chromosome 14 in common but not to a hybrid that contains only chromosome 8 (Fig. 3), confirming the derivation of pSKW 1.4X from chromosome 14. Both pSKW 1.4X probe and 3′ *myc* probe pCA 1.7S detected a 5.2-kb Eco RI fragment by Southern blot analysis, confirming that both probes are located on the same rearranged restriction fragment. The fact that pSKW 1.4X probe does not detect a germline DNA fragment in SKW-3 (Fig. 3) is in agreement with the cytogenetic observation that the normal chromosome 14 is missing in this cell line (*6*). Therefore the recombinants containing the rearranged c-*myc* locus resulted from the t(8;14) and not from a rearrangement of chromosome 8 sequences.

A partial restriction map for >50 kb of the TCR-α locus is shown in Fig. 2C. Comparison of the restriction map of the SKW-3 rearranged clones and the germline J_α region shows that the restriction map 3′ of the breakpoint is identical to the restriction map of a cloned DNA segment located 36 kb 5′ to the TCR-α constant region (Fig. 2, B and C). Homology with this region was demonstrated by cross-hybridization of pSKW 1.4X with the appropriate restriction fragments in a genomic clone that covers this region of the germline TCR-α locus. Since the orientation of both c-*myc* and the TCR-α locus on their respective chromosomes is already known we can conclude that the translocation in SKW-3 involves a similar head-to-tail rearrangement as ob-

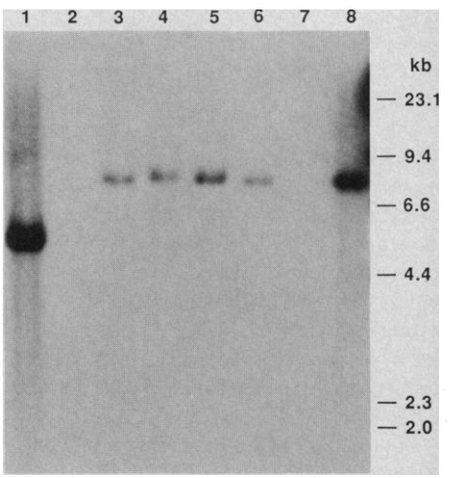

Fig. 3. Southern blot hybridization with the pSKW 1.4X probe of Eco RI–digested DNA's from human cells and human cells × rodent cells containing chromosomes 8 or 14. Lane 1, SKW-3 DNA; lane 2, 706B6-40 C1 17 hybrid DNA containing only human chromosome 8 (*4*); lane 3, 3a hybrid DNA containing human chromosomes 9, 12, 13, 14, 17, and 22 (*23*); lane 4, GL3 hybrid DNA containing human chromosomes 4, 6, 7, 13, 14, 17, 18, and 20 (*23*); lane 5, M44 C1 2S5 hybrid DNA containing the 14q+ chromosome of P3HR-1 Burkitt lymphoma with the t(8;14)(q24;q32) translocation. The breakpoint on chromosome 8 is 5′ of the c-*myc* gene (*4*); lane 6, 52-63 C1 7S17 hybrid DNA containing the 14q+ chromosome of KOP-2 cells, which have a t(14;X)(q32;q13) (*4*); lane 7, LMTK$^-$ mouse DNA; lane 8, 697 DNA.

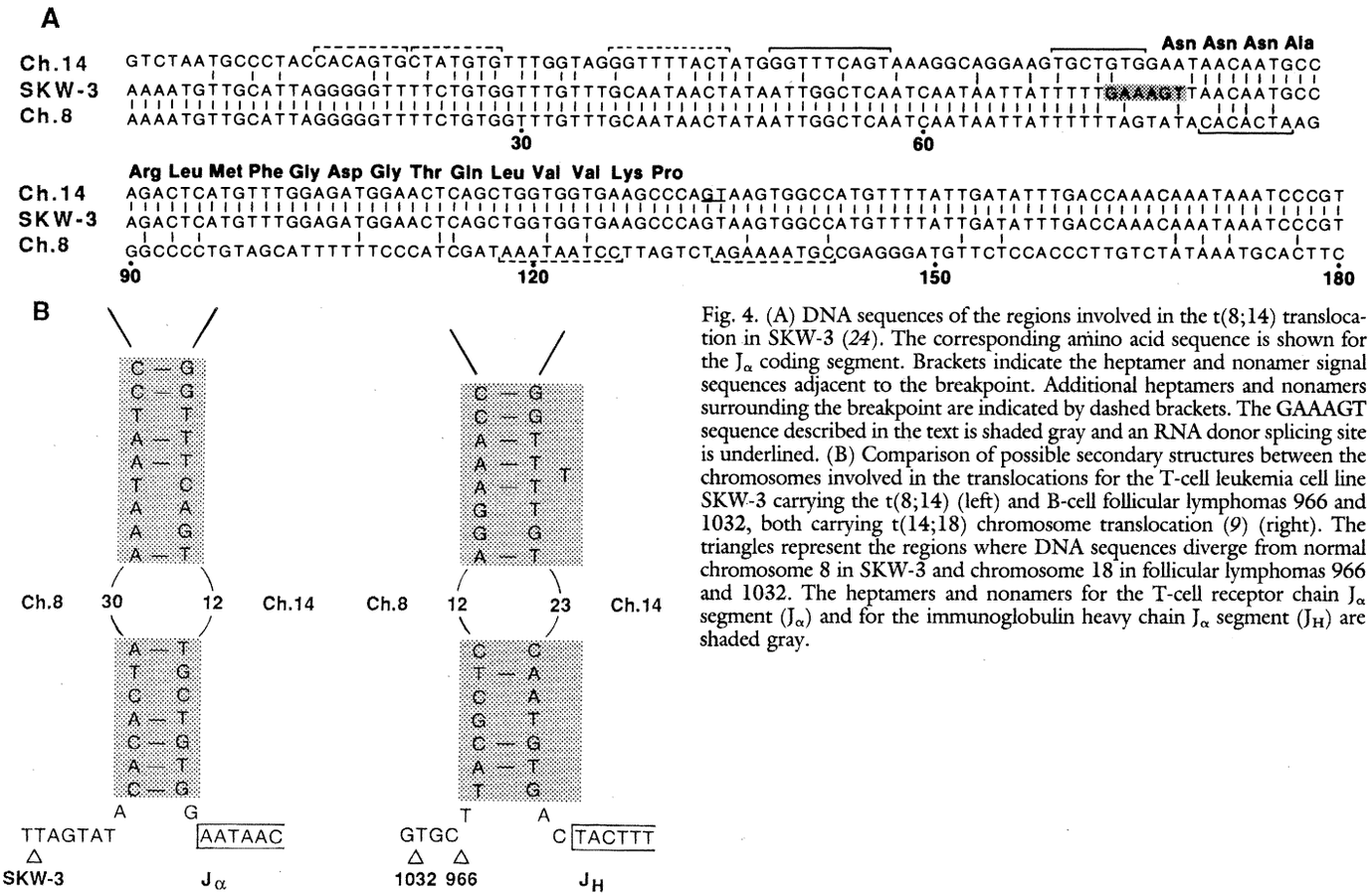

Fig. 4. (A) DNA sequences of the regions involved in the t(8;14) translocation in SKW-3 (*24*). The corresponding amino acid sequence is shown for the J_α coding segment. Brackets indicate the heptamer and nonamer signal sequences adjacent to the breakpoint. Additional heptamers and nonamers surrounding the breakpoint are indicated by dashed brackets. The GAAAGT sequence described in the text is shaded gray and an RNA donor splicing site is underlined. (B) Comparison of possible secondary structures between the chromosomes involved in the translocations for the T-cell leukemia cell line SKW-3 carrying the t(8;14) (left) and B-cell follicular lymphomas 966 and 1032, both carrying t(14;18) chromosome translocation (*9*) (right). The triangles represent the regions where DNA sequences diverge from normal chromosome 8 in SKW-3 and chromosome 18 in follicular lymphomas 966 and 1032. The heptamers and nonamers for the T-cell receptor chain J_α segment (J_α) and for the immunoglobulin heavy chain J_α segment (J_H) are shaded gray.

served for the variant Burkitt lymphoma with the t(2;8) and t(8;22) chromosome translocations (*12, 13*).

The nucleotide sequences surrounding the SKW-3 breakpoint and the corresponding sequences derived from the normal chromosome 8 and the normal chromosome 14 are shown in Fig. 4A. A J_α amino acid coding segment is located at nucleotides 78 to 131 (Fig. 4A) on chromosome 14. The coding region of the J_α sequence was identified by a sequence encoding Phe-Gly-X-Gly, that is conserved in virtually all J gene segments of the T-cell receptor (*14–16*). The 3′ boundary of the J_α segment was identified by a proper donor splice site for joining the J_α to the C_α RNA sequence (*15–17*). Immediately 5′ of the J_α element are sequences that have homology to the heptamer and nonamer recombination signals (*18*) separated by an appropriate 12-nucleotide-long spacer. A second nonamer is indicated just 5′ of the first, which is 24 bp from the heptamer. The joining signals in this region would appear to be capable of interacting with both one-turn and two-turn joining signals.

A single heptamer sequence that is capable of base pairing with the breakpoint heptamer on chromosome 14 is indicated just 3′ of the breakpoint on chromosome 8. While no sequences with homology to nonamers occur at the proper spacing from the heptamer on chromosome 8, there are nonamer-like sequences seen further 3′.

The nucleotide sequences for the germline regions from chromosomes 8 and 14 that are involved in the translocation are completely homologous 5′ and 3′ of the breakpoints, respectively, except for a 6-bp (GAAAGT) insert between the two joined chromosomes (Fig. 4A). We have previously suggested that the extra nucleotides at breakpoints in B-cell translocations may represent N regions (*8–9*), stretches of extra nucleotides that are presumably added by the enzyme terminal transferase (*19*) at the pre-B and pre-T cell stage of differentiation. However, an AGT and a GAA triplet can be found on chromosomes 8 and 14, respectively, at the breakpoint site (Fig. 4A) and it is possible that a reshuffling of these two triplets during the joining of the two chromosomes may have generated the 6-bp segments observed at the joining site. The illegitimate use of signal sequences for V-J joining has recently been described in conjunction with enhancer deletions in mouse plasmacytomas (*20*). The presence of an inverted heptamer at the recombination site and the observation of inserted nucleotides at the deletion recombination site have been interpreted to indicate that the machinery involved in V-J joining is at least responsible in part for the deletion event (*20*). Furthermore, recent reports describing a V_H to V_HDJ_H rearrangement that occurs via an isolated heptamer within the V_H coding sequences (*21, 22*), suggest that the heptamer alone may be sufficient for joining. Thus the molecular mechanisms involved in the chromosomal translocations observed in human B- and T-cell malignancies are remarkably similar (Fig. 4B).

The results presented in this report also indicate that the chromosome translocations involved in T-cell leukemias occur at an early stage in T-cell ontogeny. Thus chromosomal translocation may precede the productive T-cell receptor gene rearrangements. Therefore, analysis for T-cell receptor gene rearrangements may not be suitable for the detection of true tumor monoclonality. In addition, anti-idiotypic immunotherapy may leave the progenitor T cells carrying the chromosomal translocation intact, affecting the value of this therapeutic approach.

REFERENCES AND NOTES

1. F. Hecht, R. Morgan, B. Kaiser-McCaw Hecht, S. D. Smith, *Science* **226**, 1445 (1984).
2. D. L. Williams *et al.*, *Cell* **36**, 101 (1984).
3. N. Sadamori *et al.*, *Cancer Genet. Cytogenet.* **17**, 279 (1985).

4. C. M. Croce *et al.*, *Science* **227**, 1044 (1985).
5. J. Erikson, D. Williams, J. Finan, P. C. Nowell, C. M. Croce, *ibid.* **229**, 784 (1985).
6. J. Erikson *et al.*, *ibid.* **232**, 884 (1986).
7. K. Nishikura *et al.*, *Proc. Natl. Acad. Sci. U.S.A.* **80**, 4822 (1983).
8. Y. Tsujimoto *et al.*, *Nature (London)* **315**, 340 (1985).
9. Y. Tsujimoto, J. Gorham, J. Cossman, E. Jaffe, C. M. Croce, *Science* **229**, 1390 (1985).
10. L. K. Sun, L. C. Showe, C. M. Croce, *Nucleic Acids Res.* **14**, 4037 (1986).
11. A. Frischouf, H. Lehrach, A. Poustka, N. Murray, *J. Mol. Biol.* **170**, 827 (1983).
12. J. Erikson *et al.*, *Proc. Natl. Acad. Sci. U.S.A.* **80**, 7581 (1983).
13. C. M. Croce *et al.*, *ibid.*, p. 6922.
14. Y. Yoshikai *et al.*, *Nature (London)* **316**, 837 (1985).
15. A. Winoto, S. Mjolsness, L. Hood, *ibid.*, p. 832.
16. B. Arden, J. L. Klotz, G. Siu, L. E. Hood, *ibid.*, p. 783.
17. R. Breathnach and P. Chambon, *Annu. Rev. Biochem.* **50**, 349 (1981).
18. S. Tonegawa, *Nature (London)* **302**, 575 (1983).
19. S. V. Desiderio *et al.*, *ibid.* **311**, 752 (1984).
20. R. J. Aguilera, T. J. Hope, H. Sakano, *EMBO J.* **4**, 3689 (1985).
21. M. Reth, P. Gehrmann, E. Petrac, P. Wiese, *Nature (London)* **322**, 840 (1986).
22. R. Kleinfield *et al.*, *ibid.*, p. 843.
23. K. Huebner *et al.*, *Proc. Natl. Acad. Sci. U.S.A.* **83**, 3934 (1986).
24. F. Sanger, S. Nicklen, A. R. Coulson, *ibid.* **74**, 5463 (1977).
25. Supported by a grant from the National Cancer Institute, CA 39860, Outstanding Investigator Award (C.M.C.), and a National Institutes of Health Training Grant, CA 09485 (R.C.H.).

26 June 1986; accepted 30 September 1986

Long-Term Potentiation in Dentate Gyrus: Induction by Asynchronous Volleys in Separate Afferents

JONATHAN WINSON AND DENNIS DAHL

Long-term potentiation (LTP), a long-lasting enhancement of synaptic efficacy, is considered a model for learning and memory. In anesthetized rats, activation of dentate granule cells by stimulating either the medial or lateral perforant pathway at frequencies of 100 to 400 Hz produced LTP of the stimulated pathway preferentially at 400 Hz. However, hippocampal pathways do not normally fire at this high rate. Stimuli at 200 Hz were then applied to either the medial or lateral pathway separately, to both pathways simultaneously, or to the two pathways asynchronously so that the composite stimulus applied to the granule cell dendrite was 400 Hz. LTP was produced preferentially in the asynchronous condition. Thus, lower frequency, physiological input volleys arriving asynchronously at medial and lateral synapses can induce LTP by activating a 400-Hz sensitive mechanism capable of integrating spatially separated granule cell inputs. This may reflect how LTP is normally produced in the dentate gyrus.

LONG-TERM POTENTIATION (LTP) of synaptic efficacy in the hippocampal formation occurs in dentate gyrus granule cells after repetitive stimulation of the medial perforant path. Trains of stimuli applied at 10 to 100 Hz for 2 to 20 seconds produce increases in efficacy that persist for hours in anesthetized preparations and for days to weeks in freely moving animals (*1*). LTP is most reliably elicited by stimuli applied at 400 Hz (*2*); trains of pulses at this frequency are currently utilized for the induction of LTP in this structure (*3*).

The physiological relevance of such stimuli depends on whether such trains of action potentials with interspike intervals of 2.5 msec are normally propagated in the hippocampal formation. Pyramidal cells of the CA1 and CA3 fields do fire in rapid, short bursts of 2 to 7 action potentials termed complex spikes (*4*). Such bursts might be capable of inducing LTP in their target areas in the hippocampal formation. However, interspike intervals of 2.5 msec or less occur infrequently (*5*). The firing rates of the cells of the entorhinal cortex which, via the medial and lateral perforant pathways, constitute the input to the dentate gyrus are unknown. However, the granule cells themselves do not exhibit complex spikes and fire at a rate of less than 100 Hz (*6*). Thus, physiological firing of hippocampal pathways as currently known does not generally reach 400 Hz. In our study we have quantified the relative efficacy of 400-Hz stimulation of the dentate gyrus in inducing LTP, and ascertained how this high frequency effect might be realized in normal animals by asynchronous inputs of lower frequency acting upon separate regions of the granule cell dendrite.

In urethane-anesthetized rats, a recording electrode was lowered to the granule cell layer of the dentate gyrus and stimulating electrodes were positioned to activate both the medial and lateral perforant pathways. The medial and lateral perforant pathways are distinct pathways that originate in different subfields of the entorhinal cortex (*7*) and innervate separate regions of the granule cell dendritic tree (Fig. 1). The two pathways may be clearly differentiated physiologically by their middle third field responses (Fig. 1, left). When we recorded in the middle third region of the dendrites (position 2), a single pulse applied to the medial perforant path resulted in a negative potential at a latency of approximately 2 msec. This is termed the evoked synaptic potential (ESP) and is a measure of the flow of current into the dendrite as a result of synaptic activity. At position 3, the positive potential (designated "a") reflects the corresponding outward flow of current from the cell body. A sufficiently high intensity of stimulation of the medial pathway elicits a population spike ("c"), which constitutes a measure of the number of granule cells firing action potentials. Stimulation of the lateral perforant path elicits an ESP in the outer region of the dendrites (position 1) at a somewhat longer latency (see below). The corresponding ESP at the cell layer is designated "b." Lateral path stimulation, even at saturation intensities, fails to elicit a population spike. A distinguishing feature of the comparative field responses is that at the level of maximum negative ESP of the medial pathway (position 2), the lateral ESP has reversed to a positivity. In these experiments, as in previous studies in the dentate gyrus (*8*), the slope of the ESP at the cell body layer is utilized as a measure of synaptic efficacy.

In all experiments it was first verified that the medial and lateral perforant paths were being stimulated separately (*9*). We recorded in the granule cell layer to determine input-output curves for the slope of the ESP for both the medial and lateral pathways and, in some cases, the amplitude of the population spike of the medial response (Fig. 2B, baseline). The effect of the frequency of stimulation on the induction of LTP was determined by testing either the medial or the lateral pathway in a given rat. In each animal a perforant path (PP) current for tetanic stimulation (LTP current) was selected slightly above that required to elicit a threshold response. The objective was to choose a current sufficiently low such that LTP would not be induced at any frequency between 100 and 400 Hz. A test current, approximately two-thirds of the saturation current, was chosen to test for the induction of LTP. The test current (a single 250-μsec pulse) was applied at 1-minute intervals for 10 minutes to establish a baseline response, and for 20 minutes after each application of

Rockefeller University, 1230 York Avenue, New York, NY 10021.